Journal of MATERIALS RESEARCH

Article
DOI:10.1557/s43578-023-01010-z

# Fabrication of silver and strontium co-loaded chitosan–gelatin nanocomposite coatings with balanced antibacterial and osteogenic properties

Dan Huang[1,3,4,5,b)], Fushi Wang[1,6,b)], Yinghui Hu[1,7], Ke Song[3,4,5], Chuanzi Liu[1], Tao Jiang[1,2,a)], Yining Wang[1,2,a)]

[1] The State Key Laboratory Breeding Base of Basic Science of Stomatology (Hubei-MOST) and Key Laboratory of Oral Biomedicine Ministry of Education, School and Hospital of Stomatology, Wuhan University, Wuhan, China
[2] Department of Prosthodontics, Hospital of Stomatology, Wuhan University, Wuhan, China
[3] Department of Stomatology, Tongji Hospital, Tongji Medical College, Huazhong University of Science and Technology, Wuhan, China
[4] School of Stomatology, Tongji Medical College, Huazhong University of Science and Technology, Wuhan, China
[5] Hubei Province Key Laboratory of Oral and Maxillofacial Development and Regeneration, Wuhan, China
[6] Department of Cariology and Endodontics, Hospital of Stomatology, Wuhan University, Wuhan, China
[7] Department of Oral Implantology and Prosthodontics, Shenzhen Stomatology Hospital Affiliated to Shenzhen University, Shenzhen, China
[a)] Address all correspondence to these authors. e-mails: jiangtao2006@whu.edu.cn; wang.yn@whu.edu.cn
[b)] These authors have contributed equally to this work.

Received: 19 January 2023; accepted: 31 March 2023; published online: 16 May 2023

**To impart balanced antibacterial and osteogenic properties to titanium substrates, we prepared silver (Ag) and strontium (Sr) co-loaded chitosan–gelatin (CSG) coatings by dual-sourced electrophoretic deposition method, producing a series of Ag/Sr-CSG-modified implants. Physicochemical study confirmed that both Ag and Sr ions were deposited into the coatings successfully. The coatings showed nanostructure, and nanoparticles could be released from the coatings. In vitro antibacterial study showed that all coatings have antibacterial activity, and as the concentration of Ag increased, the corresponding antibacterial ability improved. In the cellular study, promoted osteogenic activity was observed on Ag1/Sr10 and Ag1/Sr50 groups, and this effect of Ag1/Sr50 group was more prominent. In total, the Ag1/Sr50 group had desirable balanced antibacterial and osteogenic properties. This study demonstrated that multiple elements could be co-loaded into CSG coatings with their functional effects preserved, and the antibacterial and osteogenic property could be balanced by adjusting the elements dosage.**

## Introduction

Biomaterials, which have been employed to augment body functions or replace damaged tissues for the past several thousand years, have greatly improved the living quality of aged or injured individuals [1]. Common examples include joint arthrodesis, fracture fixation, and implants in dentistry [2]. Moreover, this field has caused huge economic benefits, among them, the number of orthopedic implants is extremely high [3]. With an increasing aging population and the desire for an active lifestyle, the demand for such implants is continuous to increase.

Currently, 70–80% of implant materials are fabricated from titanium, which possess excellent biocompatibility, corrosion resistance, and mechanical robustness [4, 5]. Although titanium implants have achieved great success, implant-associated infections still constitute a global health concern and could cause serious consequences [6–8]. The infections are often recurrent, expensive to treat, associated with high rates of morbidity, and will increase the burden of patients both physiologically and economically [9]. To reduce the infections, it has motivated the development of novel strategies to modify implant surface and design antibacterial coatings [10–12]. Antibacterial compounds (e.g., antibiotics, metal ions, organic molecules) are used in active coatings to down-regulate infection [13]. Among the diverse metal elements, silver (Ag) is one of the most commonly employed elements in antibacterial surface procedures, for its high antibacterial

activity and minimal bacterial resistance [14, 15]. However, the desired antibacterial activity often compromises the biocompatibility. Researchers have demonstrated that the higher the content of Ag ions loaded on the substrate, the better the antibacterial effect, but the corresponding biocompatibility was decreased, and it may be cytotoxic when Ag concentration exceeds a certain threshold [16, 17]. A feasible strategy to alleviate its potential cytotoxicity while preserving its optimal antibacterial activity is incorporating a secondary bioactive agent [18, 19].

One of the suitable binary elements to incorporate into an Ag-loaded titanium substrate is strontium (Sr), which has bone-seeking behavior and has already been used in clinic to prevent and treat osteoporosis [20, 21]. Strontium can promote osteoblastogenesis, matrix mineralization, and calcium nodule formation by upregulating the expression of osteogenic genes. Meanwhile, Sr inhibits bone resorption by inhibiting osteoclast maturation and survival [22, 23]. Therefore, Sr is deemed to be effective to enhance the bioactivity and biocompatibility of material [24]. In addition, researchers have found that Sr could compete with Ag for binding sites specific to cellular function, thereby reducing cytotoxicity of Ag [25, 26]. Thus, the incorporation of Sr into the Ag-loaded material may offset their potential cytotoxicity. In total, the Ag/Sr-containing titanium substrate may have osteogenic activity except for reducing bacterial infections.

In our previous study, we have chosen electrophoretic deposition (EPD) from various methods to modify titanium substrate owing to its advantages of short formation time, simple apparatus, and easy control of deposited film [27]. Through EPD, we have fabricated biodegradable chitosan–gelatin (CSG) coating on titanium, and the coating has osteogenic property with a three-dimensional porous scaffold-like structure [28, 29]. In addition, the CSG coating was a promising candidate for further loading of functional agents. We have incorporated Ag and Sr into the CSG coatings individually, and demonstrated that the coatings have remarkable antibacterial and osteogenic property, respectively [30, 31]. However, the Ag and Sr co-loaded CSG coatings have not been investigated yet. In addition, in order to get satisfactory Ag/Sr co-loaded coatings, the suitable dosage of these two elements also needs to be explored.

Therefore, in the present study, we prepared a set of Ag/Sr-CSG coatings with different amounts of Ag and Sr co-loaded via EPD, and investigated whether the overall performance of the implants could be balanced by adjusting the elements dosage. We expect that the incorporation of Sr can alleviate the potential cytotoxicity of Ag, while maintaining its optimal antibacterial activities, and the composite Ag/Sr-CSG coatings may have desirable balanced antibacterial and osteogenic properties. This study may demonstrate that multiple elements could be co-loaded into CSG coatings with their functional effects preserved, and highlight the potential of Ag/Sr-CSG coatings for use in clinical applications.

## Results and discussion

### Deposition mechanism of Ag/Sr-CSG coatings

Associated infection and lack of native tissue integration are the most common causes of failure of orthopedic implants [32]. To address these challenges, attempts have been made to modify titanium substrates [33, 34]. In this study, a series of Ag/Sr-doped CSG coatings were applied to the titanium implants to modify them. The implants gained balanced antibacterial and osteogenic properties as a result.

EPD was chosen to prepare the coatings because of its mild deposition conditions, and CSG coatings were used as platforms for loading functional elements. As mentioned in our previous study [29], chitosan could be dissolved in acidic HCl solution due to protonation of its amino groups. Once gelatin was dissolved in chitosan solution, chitosan–gelatin (CSG) complexes were formed by electrostatic interaction between -$NH_3^+$ groups on chitosan and –$COO^-$ groups on gelatin. When Silver nitrate and Strontium nitrate solutions were added into CSG suspension, stable colloid system of Ag/Sr-CSG complex was formed via chelation and electrostatic attraction between Ag/Sr and chitosan [35]. As shown in Table 1, the zeta potential value of EPD solutions were all above + 50 mV with no significant difference. As reported by literature, a minimum potential of 30 mV is required to obtain a physically stable suspension [36]. So, all the composite EPD solutions achieved a good physical stability. The suspended complex in the solutions displayed a high and uniform surface charge, thus facilitating the EPD process [27].

When the charge was applied, the positively charged Ag/Sr-CSG complex was attracted and moved to the cathode. The pH value near the cathode rose up to approximately 10 due to the following reaction: $2H_2O + 2e^- \rightarrow H_2\uparrow + 2OH^-$ [27, 37]. Consequently, chitosan experienced a higher pH than p$K_a$ and became insoluble around the cathode. Therefore, Ag/Sr-CSG complex was deposited on the titanium substrate together with chitosan. As for the anode, the oxygen gas was produced owing to the oxidation reaction: $2H_2O - 4e^- \rightarrow O_2 + 4H^+$ [38]. The metal activity of strontium is stronger than silver, so silver is more easily to be reduced during EPD [39]. In the alkaline environment near the

**TABLE 1:** Zeta potential of all four groups of EPD solutions at Ph = 4 ($n$ = 5).

| Sample | Zeta potential (mV) | SD (mV) |
|---|---|---|
| CSG | 50.68 | 3.43 |
| Ag1/Sr10 | 50.82 | 3.66 |
| Ag1/Sr50 | 51.62 | 3.95 |
| Ag5/Sr50 | 50.34 | 3.34 |

cathode, we inferred that $Sr^{2+}$ underwent the following reaction: $Sr^{2+} + 2OH^- \rightarrow Sr(OH)_2$, and $Sr(OH)_2$ subsequently interacted with $CO_2$ in the air, thus generating $SrCO_3$ [30]. Meanwhile, the AgCl product was produced due to the interaction between silver and chloride ions in the EPD solution ($Ag^+ + Cl^- \rightarrow AgCl$). Furthermore, a part of Ag ions was inferred to be reduced to metallic Ag, and gradually oxidized to $Ag_2O$ when exposed to air ($Ag^+ + e^- \rightarrow Ag$, $4Ag + O_2 \rightarrow 2Ag_2O$) [31].

## Physicochemical characterization of the deposited coatings

### Surface topography and microstructural characterization

As shown in Fig. 1(a–d), fluorescence images of the fresh coatings exhibited blue fluorescence due to autofluorescence of chitosan. CSG coatings showed micro-porous structure, while some microparticles distributed uniformly in the micro-porous background in Ag/Sr groups. The porous structures of all coatings were caused by hydrogen evolution at the cathode during EPD, and it has been reported that such porous structures were benefit for cell growth, migration, and nutrient flow [40]. With the increasing amount of Ag and Sr in the coatings, the number of pores decreased while the density of the microparticles increased, this was probably due to the formation of reduced metallic Ag that consumed electron, which indirectly inhibit the generation of hydrogen [41].

Under FESEM [Fig. 1(e–p)], CSG coatings showed a smooth surface morphology. With the addition of Ag and Sr, uniformly distributed micro-scale particles appeared. The density of the microparticles increased as the concentration of the ions increased. In more detail, these microparticles in Ag/Sr groups seemed to be composed of smaller nanoscale particles.

The results of EDS analysis shown in Fig. 2(a) confirmed the presence of Ag and Sr in all Ag/Sr coatings. In addition, a higher concentration of Ag and Sr in the EPD solution led to a relatively higher concentration of Ag and Sr in the coatings. The corresponding EDS mapping analysis [Fig. 2(b)] revealed that Ag and Sr were distributed uniformly on the surface, indicating homogeneous dispersion of the doped element in the coatings. In addition, the dot density variation of the doped elements in Ag/Sr coatings coincided with the results of EDS analysis. As displayed in Fig. 2(c), XRD patterns of control CSG group showed diffraction peaks of chitosan and the titanium substrates. In Ag5/Sr50 group, the XRD patterns displayed the peaks of strontium carbonate ($SrCO_3$, $2\theta = 25.2°$, 26.5°, 44°) and the peaks of silver chloride (AgCl, $2\theta = 27.8°$, 32°, 46°). These results confirmed the above speculation about the generation of $SrCO_3$ and AgCl during EPD process [42, 43]. But all coatings did not show the peaks of $Ag_2O$, the Ag1/Sr50 group only showed the

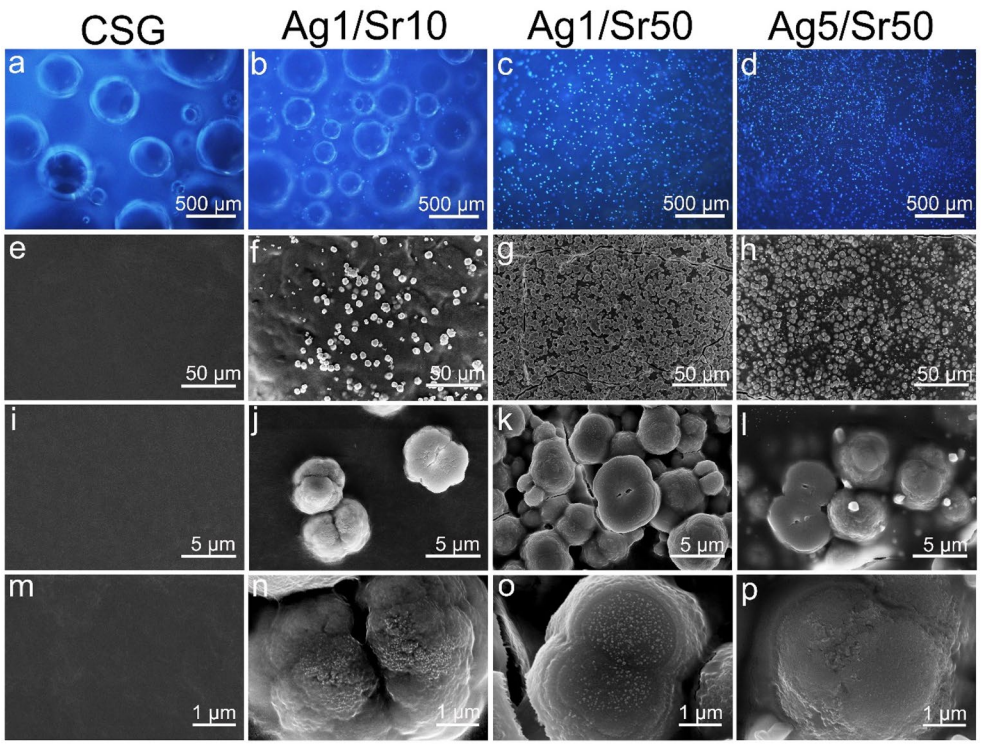


**Figure 1:** Fluorescence images of the coatings (a–d); and FESEM morphology of the coatings: low magnification (e–h), high magnification (i–p).

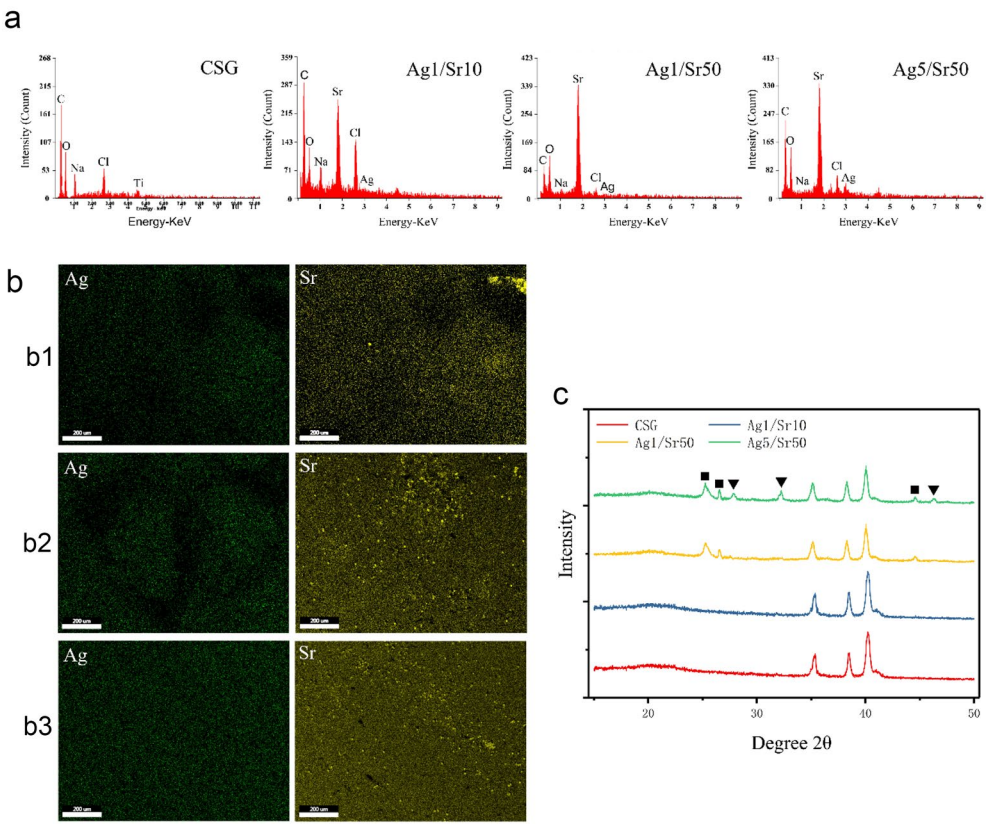


**Figure 2:** (a) EDS of the coatings; (b) EDS mapping of the Ag/Sr coatings for Ag and Sr: (b1) Ag1/Sr10, (b2) Ag1/Sr50, (b3) Ag5/Sr50; (c) XRD patterns of the coatings (black square-peaks: SrCO3, black down-pointing triangle-peaks: AgCl).

diffraction peaks of $SrCO_3$ but not AgCl, and the patterns of Ag1/Sr10 reflect no difference compared with CSG group. These were all probably due to the low content of these metallic compounds, and some more sensitive detection methods were needed in the follow-up study.

## Metal ions entrapment and release study

Figure 3(a, b) displays the amount of Ag and Sr entrapped in each group increased as their concentration in the EPD solution ascended. The entrapment of metal ions was partly due to EPD and partly because of physical adsorption.

In the release assay [Fig. 3(c, d)], all Ag/Sr groups presented a bi-phasic release of Ag/Sr with an initial burst release in the early 24 h [44], which may be attributed to Ag/Sr on the surface layers of the coatings. A reduced release rate was observed subsequently, owning to the physical degradation of the coatings. The burst release could ensure a local high drug concentration in the early stage, which prevented low topical drug concentration and side effects of systemic administration. The release of Ag was still observed at the end of the experiment in all Ag/Sr groups, while sustained release of Sr was only observed in Ag1/Sr50 and Ag5/Sr50 groups, and the release of Sr ended on the third day for Ag1/Sr10 group.

TEM images [Fig. 3(e)] showed the morphology of the nanoparticles released from the coatings. These nanoparticles were uniformly distributed with diameters of 5–50 nm, and there was no apparent difference among the groups. The EDS mapping images [Fig. 3(f)] indicated that these nanoparticles contain well-dispersed Ag and Sr elements in Ag/Sr groups. What is more, the dot density variation coincided with the results of the EDS mapping analysis of the deposited coatings. These results suggested that Ag and Sr were released from the coatings. The use of nanocarriers for drug delivery was reported to improve the therapeutics' solubility, extended their half-life, and reduce their immunogenicity [45, 46]. Therefore, compared with traditional hydrogel and polymer coatings that could not release nanoparticles, the Ag/Sr-CSG coatings might be considered as an advanced and promising surface functionalization strategy. Considering the result of FESEM with TEM, we inferred that nanoparticles were formed in EPD process, which underwent aggregation and developed into microparticles as shown in FESEM images [Fig. 1(e–p)].

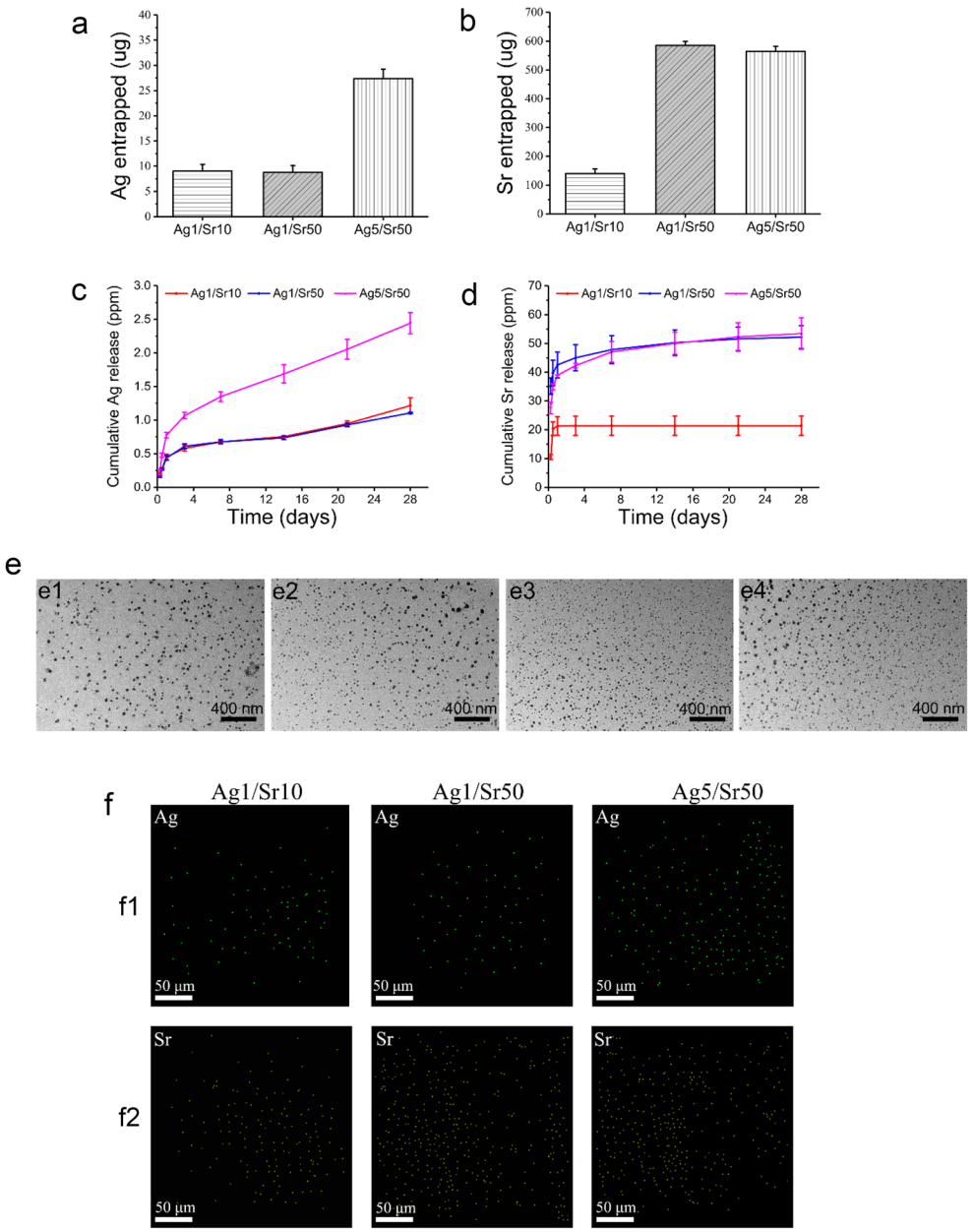


**Figure 3:** (a) Ag and (b) Sr entrapment of the Ag/Sr coatings; Cumulative release profiles of (c) Ag and (d) Sr released form Ag/Sr coatings in PBS; TEM images of the released nanoparticles: (e1) CSG, (e2) Ag1/Sr10, (e3) Ag1/Sr50, (e4) Ag5/Sr50; EDS mapping of the particles released from the Ag/Sr coatings: (f1) Ag, (f2) Sr.

## Degradation rate

As shown in Fig. 4(a), the weight of the coatings decreased significantly in the first three days, followed by relatively little change in the following days. Generally speaking, the weight loss rate decreased as the amount of the metal ions in the coating increased. This result could be attributed to the large electrostatic potential gap of the Ag/Sr-CSG coatings, which could consequently improve the stability of the coatings and decrease degradation rates [47].

## Mechanical properties

As displayed in Fig. 4(b), the tensile bond strength of the coating increased when the metal ions were introduced, and significant difference could be observed between the CSG group and the Ag5/Sr50 group. As for the shear bond strength, there was no statistical difference among all the groups [Fig. 4(c)]. The mechanical property study revealed that the incorporation of ions could improve the bonding strength of the coatings. In our previous study [28], even the pure CSG coating could withstand

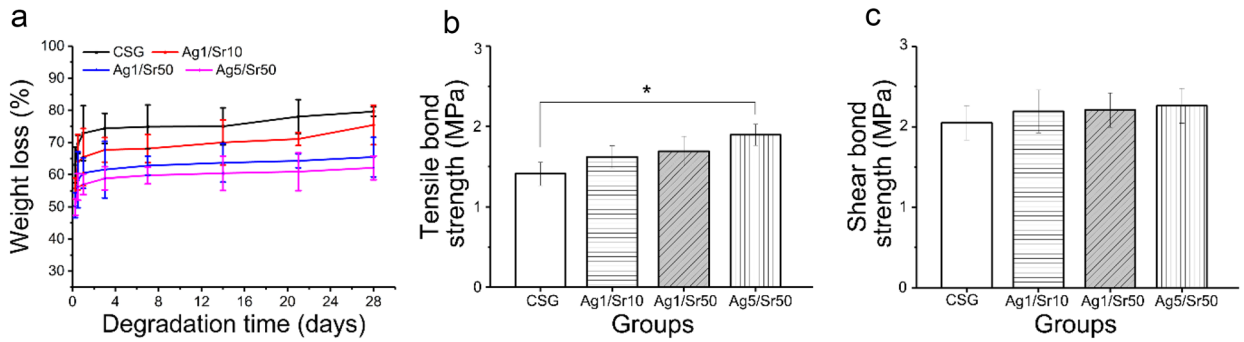


**Figure 4:** (a) Degradation rate of the coatings; (b) Tensile bond strengths; and (c) Shear bond strength of different coatings. $n = 3$, $^*p < 0.05$.

the interfacial stress during the implant surgery. Therefore, the Ag/Sr-CSG coatings were expected to be strong enough in clinical application.

## In vitro antibacterial study

### Observation of the bacteria by FESEM

The results of FESEM showed that the amounts of *E.coli* and *S.aureus* on the coatings were significantly decreased with the concentration of Ag increased [Fig. 5(a, b)]. Almost no bacteria were observed in Ag5/Sr50 group.

### Live/dead staining

As displayed in Fig. 5(c, d), the images of CSG group displayed almost only green fluorescent spots (live bacterial colonies) with no red fluorescent spots (dead bacterial colonies) for both *E.coli* and *S.aureus*. In the Ag1/Sr10 and Ag1/Sr50 groups, the images showed large scale of red fluorescent spots with few green spots. While in the Ag5/Sr50 group, there were only red fluorescent spots with no green fluorescent spots.

### Quantitative measurements of antibacterial ability

To quantify the antibacterial ability of Ag/Sr samples, bacteria adhered on the surface and suspended in the culture medium were counted. The density of both bacteria showed similar variation tendency: CSG group > Ag1/Sr10 group, Ag1/Sr50 group > Ag5/Sr50 group [Fig. 5(e)]. The antibacterial ratios were calculated and shown in Fig. 5(f), for *E.coli*, the Ra values of Ag1/Sr10, Ag1/Sr50 and Ag5/Sr50 group were 78.97%, 79.46% and 100%, respectively; and Rp values were 74.89%, 79.71% and 99.95%, respectively. As for *S.aureus*, the Ra values were 80.36%, 80.09%, and 99.09%, respectively; and Rp values were 67.02%, 62.81%, and 98.25%, respectively.

To deal with the problem of implant-associated infections, Ag was added into CSG coatings for its antibacterial ability. Our results demonstrated that Ag/Sr-CSG coatings revealed dual contact and release-based antibacterial activity. The coatings can kill the bacteria adhered on its surface, then prevent biofilm formation, which is the most common cause of implant-associated infection [48]. At the same time, it can inhibit the bacteria in the surrounding environment, then control the infection completely. In addition, the antibacterial effect was in a dose-dependent manner, and the content of Ag decided its antibacterial level. This antibacterial property was predominantly attributed to the release of Ag ions from the Ag/Sr-CSG complex [15, 49]. The interaction of Ag ions with thiol groups of vital enzymes and proteins affects cellular respiration and the transport of ions across membranes, ultimately resulting in cell death [50, 51]. Meanwhile, it was reported that the AgCl product could inhibit microbial growth depending on the particle size and bioavailability [52]. It was worth noting that Gram-negative bacteria were shown to be more sensitive to the release-based antibacterial mode compared with Gram-positive bacteria. This was probably due to the fact that positive charged Ag ions are electrostatically attracted to the cell walls of negatively charged bacterial cells, and the localized concentration of Ag ions is significantly improved. Therefore, the corresponding antibacterial effect was higher for *E.coli* compared with *S.aureus*.

## In vitro cellular study

### Cell adhesion and morphology

Although Ag ions have outstanding antibacterial property, its potential cytotoxicity always limit its application. To alleviate this potential cytotoxicity, Sr was added into the coating as a binary element, for it can both stimulate bone formation and inhibit bone resorption [20, 21]. To get desirable balanced antibacterial and osteogenic properties, we prepared a set of Ag/Sr-CSG coatings with different proportions of Ag and Sr loaded.

FESEM images revealed that CSG, Ag1/Sr10, and Ag1/Sr50 samples could support extensive cell attachment and spreading [Fig. 6(a)]. In addition, extended filopodia of

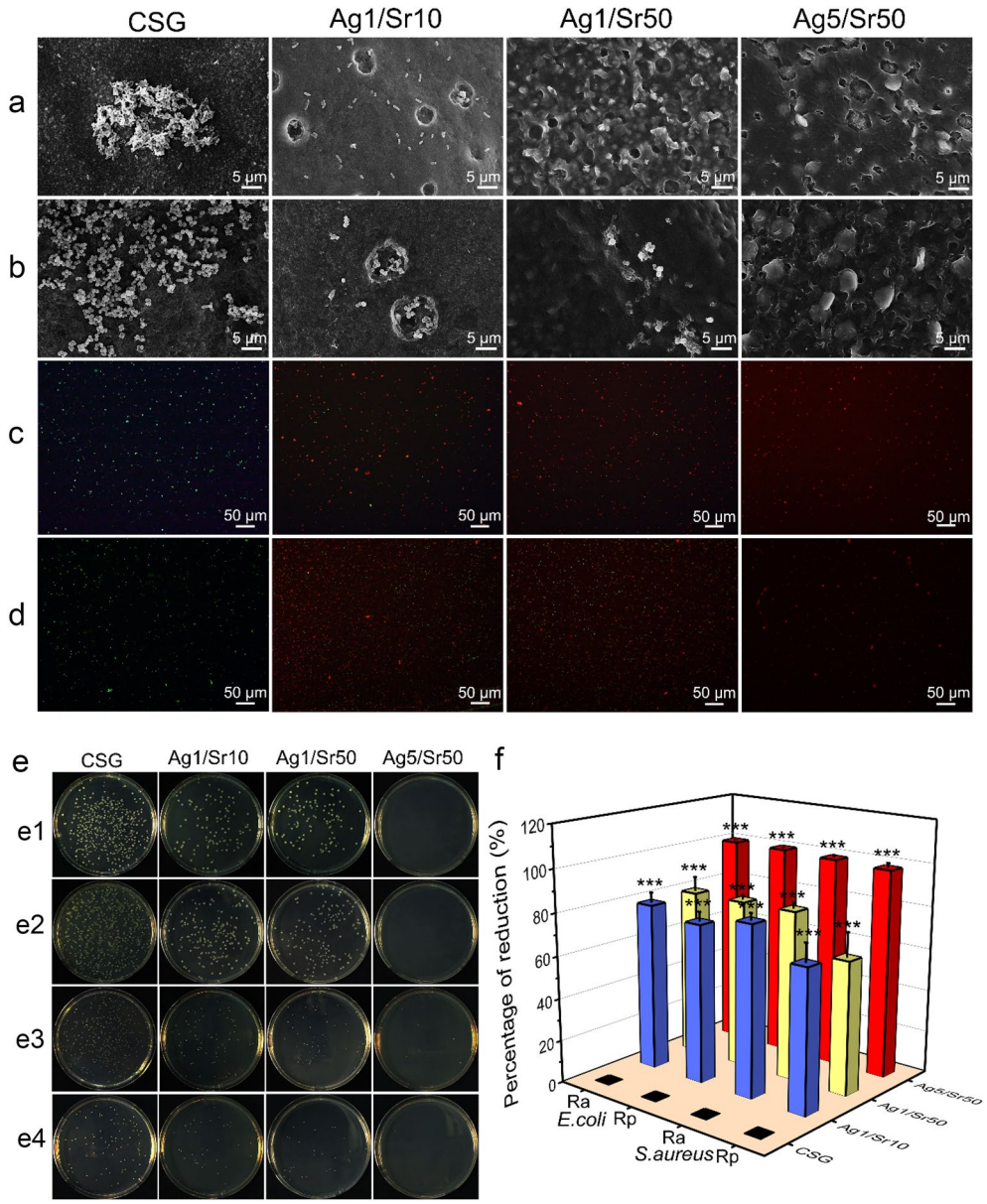


**Figure 5:** FESEM morphologies of (a) *E.coli* and (b) *S.aureus* adhered on the deposited coatings; Live/Dead stain fluorescent images of (c) *E.coli* and (d) *S.aureus* after dyeing with SYTO 9 and PI; Typical photographs of recultivated bacterial colonies on agar: (e1) *E.coli* and (e3) *S.aureus* adhered on the surface, (e2) *E.coli* and (e4) *S.aureus* suspended in the medium; (f) Corresponding antibacterial ratios of Ra and Rp. $n = 3$, $^{*}p < 0.05$, $^{**}p < 0.01$, $^{***}p < 0.001$ *vs* the CSG group.

BMSCs were connected with the microparticles on the coatings. While in Ag5/Sr50 group, only cell debris could be observed. As for cytoskeleton staining assay [Fig. 6(b)], cell density of CSG, Ag1/Sr10, and Ag1/Sr50 groups showed no obvious difference, and the cell all displayed polygonal shape with interconnected filopodia. The same as FESEM, the Ag5/Sr50 sample only showed little deformed cell debris under fluorescence microscopy.

### Cell proliferation

It is observed that cell population of all groups increased from day 1 to 7 with the exception that the cell on Ag5/Sr50 coatings did not show normal proliferation [Fig. 6(c)]. In general, Ag1/Sr10 and Ag1/Sr50 group manifested higher cell activity than CSG group, while cell activity of Ag5/Sr50 group was significantly lower than the other groups. These suggested that Ag1/

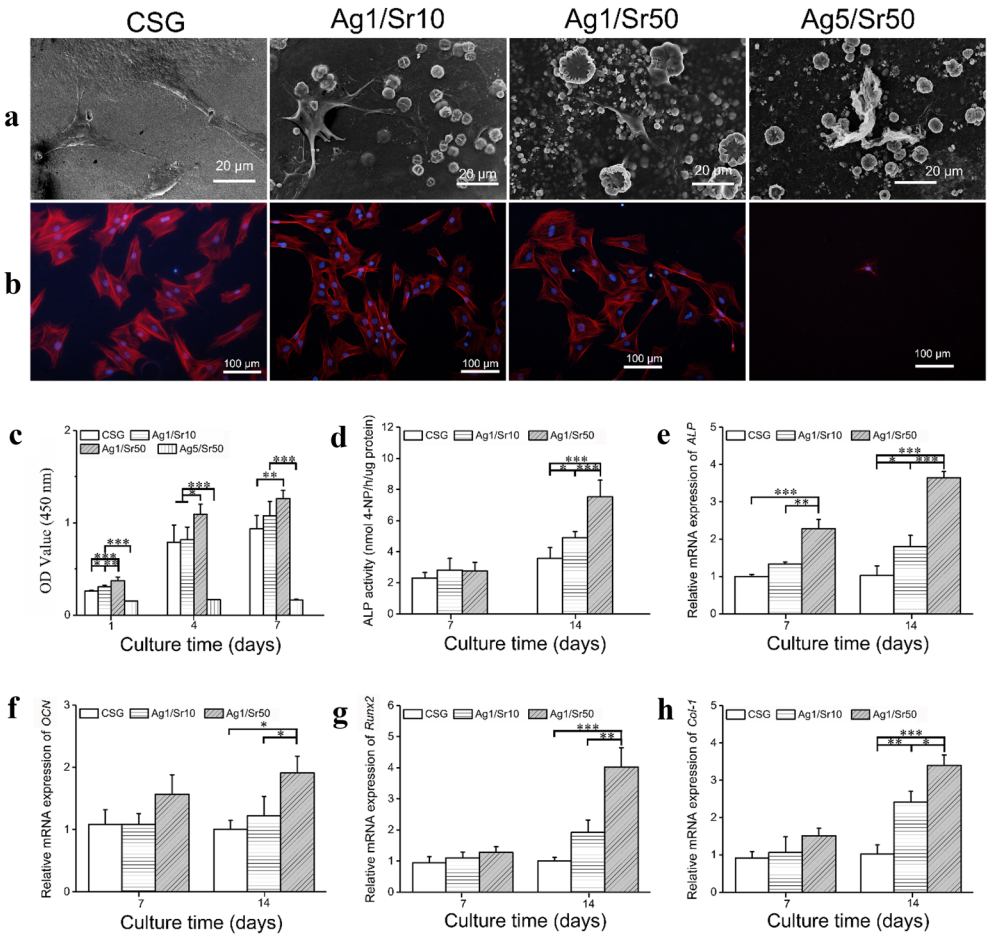


**Figure 6:** (a) FESEM images and (b) Fluorescence images of BMSCs after 1 day of culture; (c) Cell viability of BMSCs cultured at specific time intervals; (d) ALP activity and gene expression levels of osteogenesis-related markers: (e) *ALP*, (f) *OCN*, (g) *Runx2*, (h) *Col-1* in BMSCs cultured with various samples at specific time intervals. $n = 3$, $^{*}p < 0.05$, $^{**}p < 0.01$, $^{***}p < 0.001$.

Sr10 and Ag1/Sr50 groups can promote cell proliferation, while the Ag5/Sr50 group had significant cytotoxicity due to excessive dosage of Ag. Therefore, the Ag5/Sr50 group had no corresponding results in the following cellular study.

### Cell osteogenic differentiation

The results in Fig. 6(d) reveal that the ALP activity of Ag1/Sr10 and Ag1/Sr50 groups were significantly enhanced on the 14th day compared with control group. In addition, the value of Ag1/Sr50 group was obviously higher than Ag1/Sr10 group.

As displayed in Fig. 6(e–h), the results showed that the expression level of osteogenesis-related genes increased in the order CSG, Ag1/Sr10, and Ag1/Sr50 group. *ALP* and *Col-1* expression levels of Ag1/Sr10 group were significantly increased compared with the control CSG group on 14th day. Moreover, the expression levels of all genes in Ag1/Sr50 group were dramatically higher than the other two groups, especially on the 14th day.

The results of ALP activity and RT-PCR showed that the osteogenic differentiation of BMSCs on the Ag1/Sr10 and Ag1/Sr50 coatings increased as the Sr entrapment ascended. These results confirmed the bone-seeking activity of Sr ions released from the coatings, and this ability was in a dose-dependent manner in certain concentration range. Researchers have found that Sr concentration between $10^{-5}$ and $10^{-4}$ M were considered the most effective to induce the osteogenic effect on primary bone cells [53], the concentration of Sr released from the coatings in the present study were actually within this range. Strontium was deemed to increase osteoblast replication, differentiation, and bone matrix mineralization probably via a calcium sensing receptor (CaR)-dependent mechanism. In addition, Sr has also been reported to direct the MSCs to the bone lineage via the Wnt/β-catenin and MAPK pathways, while simultaneously repress their commitment to other lineages such as adipocytes [54].

The loading amount of Ag and Sr are both crucially important for the overall performance of Ag/Sr-CSG coatings. As for

the three Ag/Sr groups in this study, the Ag1/Sr10 group had a certain degree of antibacterial property, but its osteogenic ability was less than the Ag1/Sr50 group; Ag5/Sr50 group had better antibacterial effect, but non-expected cytotoxicity occurred; only Ag1/Sr50 group displayed better osteogenic behavior while maintaining its sufficient antibacterial activity. In the Ag1/Sr50 group, both the Ag and Sr ions exhibited ideal effect, ensuring the desirable balanced antibacterial and osteogenic properties of the coatings.

## Conclusion

In this study, a series of Ag/Sr-CSG coatings with different proportions of Ag and Sr introduced were prepared via EPD technique. The results showed that multiple metal ions could be co-loaded into CSG coatings with their functional effects preserved. By controlling the dosage of the metal elements, the Ag1/Sr50 coatings displayed excellent balanced antibacterial ability and osteogenic activity in vitro without cytotoxicity. These properties would make the Ag1/Sr50-CSG coating a promising candidate for surface modification of biomedical materials, although study on the galvanic effect between these two metal ions and further in vivo study are needed.

## Materials and methods

### Materials

Pure titanium disks (diameter: 15 mm; thick: 1 mm) were provided by Baoji Titanium Industry Co., Ltd and pretreated by sandblasted, acid-etched, and ultrasonically cleaned before use. Chitosan (Mw 1,000,000, deacetylation degree > 95%, Golden-Shell Biomedical Co., Ltd.) and type A gelatin (Sigma, G1890) were used.

### Preparation of the electrophoretic solutions and samples fabrication

According to our previous study, the CSG solution was prepared by dissolving 0.6 g chitosan and 1.4 g gelatin in 80 ml HCl (0.04 M) solution. The pH value was adjusted to 4.0 using NaOH solution, and the total volume was brought to 100 ml with Milli-Q water. Sliver nitrate and Strontium nitrate were added into CSG solution in a dose-dependent manner. The final concentration of Ag and Sr ions in each group is shown in Table 2. To evaluate the stability of the EPD solution, the zeta potential was measured by photon correlation spectroscopy (Zetasizer 3000, Malvern Instruments, UK).

During EPD process, titanium substrate was used as cathode and a parallel platinum plate as anode, with 50 mm distance between them. A direct current power supply (Model 6614C, Agilent Technologies, China) was applied to connect the two electrodes and kept at 15 mA for 2 min. After deposition, titanium substrate was removed from the EPD solution, and air-dried for future study.

**TABLE 2:** Concentration of chitosan, gelatin, Sliver nitrate, and Strontium nitrate in EPD solution.

| | CSG | Ag1/Sr10 | Ag1/Sr50 | Ag5/Sr50 |
|---|---|---|---|---|
| Chitosan (CS, g/100 ml) | 0.6 | 0.6 | 0.6 | 0.6 |
| Gelatin (G, g/100 ml) | 1.4 | 1.4 | 1.4 | 1.4 |
| Ag (mM) | 0 | 1 | 1 | 5 |
| Sr (mM) | 0 | 10 | 50 | 50 |

## Characterization of the coatings

### Surface topography and physicochemical characterization

The coatings were examined by fluorescence microscopy (Leica DM4000B, Germany) immediately after EPD, and observed by field emission scanning electron microscopy (FESEM, Zeiss, Germany) after dried. Energy-dispersive X-ray spectrometry (EDS, Quanta-200, FEI, Netherlands) was applied for qualitative elemental analysis of the coatings. Meanwhile, the Ag and Sr element distribution of the coatings was monitored by EDS elemental mapping. Crystalline state of the coatings was analyzed by an X-ray diffractometer (XRD, D8 Advance; Bruker AXS Inc., USA) using CuKD radiation.

### Ag and Sr entrapment and release assay

In ion entrapment assay, fresh coatings were collected immediately after EPD and treated with hydrogen nitrate ($HNO_3$), then atomic absorption spectrophotometer (AAS, ContrAA 700, Analytik jena, Germany) was used to analyze concentration of Ag and Sr.

In Ag/Sr release study, the dried coatings were immersed in 5 ml phosphate-buffered saline (PBS) at 37 °C. At 6 h, 12 h, 24 h, 3 days, 7 days, 14 days, 21 days, and 28 days, all the immersion solutions were collected and refilled with fresh PBS. The collected solution was pretreated with $HNO_3$ and then measured by AAS.

To observe the compounds released from the coatings, the dried coatings were soaked in 5 ml Milli-Q water for 24 h, and then the suspensions were analyzed by transmission electron microscopy (TEM, JEOL JEM 2010, JEOL Ltd., Japan). In addition, EDS elemental mapping was performed to investigate the Ag and Sr element distribution of the released particles.

## Degradation rate

Degradation of the coatings was conducted in degradation solution (sterilized PBS with 1.5 μg $ml^{-1}$ lysozyme) at 37 °C. After incubating for 6 h, 12 h, 24 h, 3 days, 7 days, 14 days, 21 days, and 28 days, the samples were removed from the solution, rinsed gently with Milli-Q water, and dried at room temperature. The same disks were put back into the degradation solution after measuring the weight. The dry weight of each pure titanium disk and coated disk were determined at the start of the study ($W_1$, $W_2$) and at each pre-determined special time interval ($W_3$). The degradation rate of the coating was calculated as follows: $D = (W_2 - W_3)/(W_2 - W_1)$.

## Mechanical properties

Instant gel adhesive was used to adhere the coating surface with another titanium plate ($20 \times 10 \times 1$ $mm^3$) or stainless steel studs (diameter: 10 mm; thick: 15 mm), and cured for 24 h at room temperature. The samples were vertically placed at the crosshead of the electrical mechanical Instron Model 4465 load frame (Instron Corporation, Norwood, MA) and the direction of applied forces coincided with the long axis of the test samples. The applied force was kept at a constant displacement of 0.5 mm per min until failure, which was identified by a drop in load.

## In vitro antibacterial study

### Observation of the bacteria by FESEM

*Escherichia coli* (*E.coli*, ATCC 25,922) and *Staphylococcus aureus* (*S.aureus*, ATCC 25,923) were used in antibacterial assay. The coated samples were cultured with 2 ml bacteria suspension with a concentration of $10^5$–$10^6$ colony-forming units $ml^{-1}$. After incubation at 37 °C for 6 h, the coatings were removed from the medium, fixed overnight at 4℃, dehydrated in an ethanol series, and then gold-sputtered in vacuum before FESEM observation.

### Live/Dead staining

For the live/dead staining assay, the bacterial solution co-cultured with the samples was stained using the Live/Dead BacLight Bacterial Viability Kits (L7012, Invitrogen, USA) and observed by fluorescence microscopy immediately.

### Quantitative analysis of the antibacterial ability

Antibacterial activity of Ag/Sr groups against both adherent bacteria and planktonic bacteria were studied. The coated samples were incubated with bacteria suspension at 37 °C for 6 h, then bacteria number in the suspension was counted by spread plate method. Meanwhile, bacteria adhered on the samples were collected by mild ultrasonication, and counted by the same method. The antibacterial ratio was measured by the following formulas: (1) Antibacterial ratio for adherent bacteria on the sample: $Ra = (A - B)/A \times 100\%$ and (2) Antibacterial ratio for planktonic bacteria in the medium: $Rp = (C - D)/C \times 100\%$. Specifically, A and B stand for the average number of bacteria adhered on the control group and Ag/Sr group, respectively, C and D represent the average number of bacteria in the medium of the control group and Ag/Sr group, respectively.

## In vitro cellular study

### Culture and expansion of rat bone marrow stromal cells (BMSCs)

Rat BMSCs were obtained from 6-week-old male Wistar rats according to the established protocols. All experimental protocols of animals in this study were approved by the Animal Care and Experiment Committee of Wuhan University, and followed the Guide for the Care and Use of Laboratory Animals of Wuhan University. Briefly, the bone marrow was quickly rinsed out with alpha minimum essential medium (α-MEM, SH30265, Hyclone, USA) containing 10% fetal bovine serum (FBS, SH30068, Hyclone, USA) and 1% penicillin–streptomycin (SV30010, Hyclone, USA), after cutting off both ends of rat femurs at the epiphysis. Cells were cultured at 37 °C in an environment of 5% $CO_2$ and passaged when reached 80–90% confluence. Only cells at passage 2–4 were used in the further study.

## Cell adhesion and cytoskeleton characteristics

BMSCs were seeded directly on the samples at a density of $2 \times 10^4/cm^2$. After one day of culture, the cells were fixed with 2.5% glutaraldehyde overnight at 4 °C, dehydrated through ethanol, and gold-sputtered in vacuum before FESEM evaluation. In the immunofluorescence assay, the cells were fixed in 4% paraformaldehyde, permeabilized by 0.3% Triton X-100, and then incubated in 1% bovine serum albumin. Afterward, rhodamine phalloidin (R-415 kit, Invitrogen, USA) and 2-(4-amidinophenyl)-6-indolecarbamidine dihydrochloride (DAPI, Invitrogen, Switzerland) were used to stain the filamentous actin and the nuclei of the cells. Immunofluorescence images were acquired using fluorescence microscopy.

## Cell proliferation

Cell counting kit-8 (CCK-8, Japan) was used to assess cell proliferation ability. After co-cultured with the samples for 1, 4, and 7 days, the cell culture plates were gently washed with PBS, and incubated with 400 μl α-MEM containing 10% CCK-8 at 37 °C

for 1 h. The absorbance value of the supernatant at 450 nm was read.

### Alkaline phosphatase (ALP) activity and real-time quantitative reverse-transcriptase polymerase chain reaction (RT-qPCR) for osteogenesis-related gene expression

In ALP activity assay, BMSCs were cultured with osteogenic medium (medium containing 10 nM dexamethasone, 10 mM β-glycerolphosphate, and 50 μg/ml ascorbic acid). After 7 and 14 days of culture, cells were lysed with 0.1% Triton X-100. Then, lysates were reacted with p-nitrophenyl phosphate in alkaline buffer solution at 37 °C for 1 h. The optical density values of the samples at 405 nm were measured, using 4-nitrophenol as standards. Finally, the ALP level was normalized to the total protein content determined using BCA protein assay.

Osteogenic differentiation of BMSCs was assessed by the expression levels of osteogenesis-related genes including *ALP*, osteocalcin (*OCN*), runt-related transcription factor 2 (*Runx2*), and type-1 collagen (*Col-1*), which were measured by RT-qPCR. At 7 and 14 days of culture, total RNA was extracted by Trizol regent, then complementary DNA (cDNA) was reverse-transcribed from 1 mg total RNA. After that, RT-qPCR was operated on Bio-Rad MyiQ single color Real-time PCR system using an SYBR Green PCR kit (Takara, Japan).

### Statistical analysis

One-way analysis of variance and post hoc Turkey testing were applied using SPSS 16.0 software to perform the statistical analysis. Symbols *, **, and *** stand for $P<0.05$, $P<0.01$, and $P<0.001$. $P$ values < 0.05 were deemed to be statistically significant.

## Acknowledgments

This work was financially supported by the National Natural Science Foundation of China (No. 81470771) and the Fundamental Research Funds for the Central Universities (No. 2042020kf0189).

## Data availability

The datasets generated during and/or analyzed during the current study are available from the corresponding author on reasonable request.

## Declarations

**Conflict of interest** There are no conflicts of interest to declare.

## References

1. C. Montoya, Y. Du, A.L. Gianforcaro, S. Orrego, M.B. Yang, P.I. Lelkes, On the road to smart biomaterials for bone research: definitions, concepts, advances, and outlook. Bone Res. **9**(1), 1–16 (2021)
2. S. Todros, M. Todesco, A. Bagno, Biomaterials and their biomedical applications: from replacement to regeneration. Processes **9**(11), 1949 (2021)
3. C. Hu, D. Ashok, D.R. Nisbet, V. Gautam, Bioinspired surface modification of orthopedic implants for bone tissue engineering. Biomaterials **219**, 119366 (2019)
4. J.S.L. Fong, M.A. Booth, A. Rifai, K. Fox, A. Gelmi, Diamond in the rough: toward improved materials for the bone-implant interface. Adv. Healthc. Mater. **10**(14), 2100007 (2021)
5. J. Quinn, R. McFadden, C.-W. Chan, L. Carson, Titanium for orthopedic applications: an overview of surface modification to improve biocompatibility and prevent bacterial biofilm formation. Iscience **23**(11), 101745 (2020)
6. E.L. Cyphert, N.J. Zhang, G.D. Learn, C.J. Hernandez, H.A. von Recum, Recent advances in the evaluation of antimicrobial materials for resolution of orthopedic implant-associated infections in vivo. Acs Infect. Dis. **7**(12), 3125–3160 (2021)
7. K.G. Neoh, X.F. Hu, D. Zheng, E.T. Kang, Balancing osteoblast functions and bacterial adhesion on functionalized titanium surfaces. Biomaterials **33**(10), 2813–2822 (2012)
8. U. Filipovic, R.G. Dahmane, S. Ghannouchi, A. Zore, K. Bohinc, Bacterial adhesion on orthopedic implants. Adv. Colloid Interfac. **283**, 102228 (2020)
9. E.C. Rodriguez-Merchan, D.J. Davidson, A.D. Liddle, Recent strategies to combat infections from biofilm-forming bacteria on orthopaedic implants. Int. J. Mol. Sci. **22**(19), 10243 (2021)
10. G. Tan, J. Xu, W.M. Chirume, J.Y. Zhang, H. Zhang, X.F. Hu, Antibacterial and anti-inflammatory coating materials for orthopedic implants: a review. Coatings **11**(11), 1401 (2021)
11. R. Kargupta, S. Bok, C.M. Darr, B.D. Crist, K. Gangopadhyay, S. Gangopadhyay, S. Sengupta, Coatings and surface modifications imparting antimicrobial activity to orthopedic implants. WIRES Nanomed. Nanobi. **6**(5), 475–495 (2014)
12. J.H. Sui, S. Liu, M.C. Chen, H. Zhang, Surface bio-functionalization of anti-bacterial titanium implants: a review. Coatings **12**(8), 1125 (2022)
13. H. Chouirfa, H. Bouloussa, V. Migonney, C. Falentin-Daudre, Review of titanium surface modification techniques and coatings for antibacterial applications. Acta Biomater. **83**, 37–54 (2019)
14. Y.A. Qing, L. Cheng, R.Y. Li, G.C. Liu, Y.B. Zhang, X.F. Tang, J.C. Wang, H. Liu, Y.G. Qin, Potential antibacterial mechanism of silver nanoparticles and the optimization of orthopedic implants by advanced modification technologies. Int J Nanomed. **13**, 3311–3327 (2018)

15. S. Chernousova, M. Epple, Silver as antibacterial agent: ion, nanoparticle, and metal. Angew. Chem. Int. Edit. **52**(6), 1636–1653 (2013)
16. U.V. Chetan, A systematic review of the interaction and effects generated by antimicrobial metallic substituents in bone tissue engineering. Metallomics **12**(10), 1458–1479 (2020)
17. M. Ramstedt, B. Ekstrand-Hammarstrom, A.V. Shchukarev, A. Bucht, L. Osterlund, M. Welch, W.T.S. Huck, Bacterial and mammalian cell response to poly(3-sulfopropyl methacrylate) brushes loaded with silver halide salts. Biomaterials **30**(8), 1524–1531 (2009)
18. X.J. He, X.Y. Zhang, L. Bai, R.Q. Hang, X.B. Huang, L. Qin, X.H. Yao, B. Tang, Antibacterial ability and osteogenic activity of porous Sr/Ag-containing TiO2 coatings. Biomed. Mater. **11**(4), 045008 (2016)
19. Y. Huang, Y.X. Zhang, M.Y. Li, H. Yang, J.Y. Liang, Y. Chen, Y.S. Zhang, X. Huang, L. Xie, H. Lin, H.X. Qiao, J.P. Lan, Physicochemical, osteogenic and antimicrobial properties of graphene oxide reinforced silver/strontium-doped hydroxyapatite on titanium for potential orthopedic applications. Surf. Coat. Tech. **446**, 128788 (2022)
20. N.J. Lakhkar, I.H. Lee, H.W. Kim, V. Salih, I.B. Wall, J.C. Knowles, Bone formation controlled by biologically relevant inorganic ions: role and controlled delivery from phosphate-based glasses. Adv. Drug Deliver. Rev. **65**(4), 405–420 (2013)
21. A. Hoppe, N.S. Guldal, A.R. Boccaccini, A review of the biological response to ionic dissolution products from bioactive glasses and glass-ceramics. Biomaterials **32**(11), 2757–2774 (2011)
22. P. Habibovic, J.E. Barralet, Bioinorganics and biomaterials: bone repair. Acta Biomater. **7**(8), 3013–3026 (2011)
23. J.Q. You, Y.D. Zhang, Y.M. Zhou, Strontium functionalized in biomaterials for bone tissue engineering: a prominent role in osteoimmunomodulation. Front. Bioeng. Biotech. **10**, 928799 (2022)
24. W. Zhang, Y. Shen, H. Pan, K. Lin, X. Liu, B.W. Darvell, W.W. Lu, J. Chang, L. Deng, D. Wang, W. Huang, Effects of strontium in modified biomaterials. Acta Biomater. **7**(2), 800–808 (2011)
25. Z. Geng, R.F. Wang, X.L. Zhuo, Z.Y. Li, Y.C. Huang, L.L. Ma, Z.D. Cui, S.L. Zhu, Y.Q. Liang, Y.D. Liu, H.J. Bao, X. Li, Q.Y. Huo, Z.L. Liu, X.J. Yang, Incorporation of silver and strontium in hydroxyapatite coating on titanium surface for enhanced antibacterial and biological properties. Mater. Sci. Eng. C Mater. Bio. Appl. **71**, 852–861 (2017)
26. Z. Geng, Z.D. Cui, Z.Y. Li, S.L. Zhu, Y.Q. Liang, Y.D. Liu, X. Li, X. He, X.X. Yu, R.F. Wang, X.J. Yang, Strontium incorporation to optimize the antibacterial and biological characteristics of silver-substituted hydroxyapatite coating. Mater. Sci. Eng. C Mater. Bio. Appl. **58**, 467–477 (2016)
27. L. Besra, M. Liu, A review on fundamentals and applications of electrophoretic deposition (EPD). Prog. Mater Sci. **52**(1), 1–61 (2007)
28. K. Ma, X. Cai, Y. Zhou, Z. Zhang, T. Jiang, Y. Wang, Osteogenetic property of a biodegradable three-dimensional macroporous hydrogel coating on titanium implants fabricated via EPD. Biomed. Mater. **9**(1), 015008 (2014)
29. T. Jiang, Z. Zhang, Y. Zhou, Y. Liu, Z.W. Wang, H. Tong, X.Y. Shen, Y.N. Wang, Surface functionalization of titanium with chitosan/gelatin via electrophoretic deposition: characterization and cell behavior. Biomacromol **11**(5), 1254–1260 (2010)
30. K. Ma, D. Huang, J. Cai, X. Cai, L. Gong, P. Huang, Y. Wang, T. Jiang, Surface functionalization with strontium-containing nanocomposite coatings via EPD. Colloid. Surface. B **146**, 97–106 (2016)
31. K. Ma, L. Gong, X. Cai, P. Huang, J. Cai, D. Huang, T. Jiang, A green single-step procedure to synthesize Ag-containing nanocomposite coatings with low cytotoxicity and efficient antibacterial properties. Int J Nanomed. **12**, 3665–3679 (2017)
32. H. Cheng, W. Xiong, Z. Fang, H. Guan, W. Wu, Y. Li, Y. Zhang, M.M. Alvarez, B. Gao, K. Huo, J. Xu, N. Xu, C. Zhang, J. Fu, A. Khademhosseini, F. Li, Strontium (Sr) and silver (Ag) loaded nanotubular structures with combined osteoinductive and antimicrobial activities. Acta Biomater. **31**, 388–400 (2016)
33. Z. Wang, B. Li, Q. Cai, X. Li, Z. Yin, B. Li, Z. Li, W. Meng, Advances and prospects in antibacterial-osteogenic multifunctional dental implant surface. Front. Bioeng. Biotech. **10**, 921338 (2022)
34. S. Kligman, Z. Ren, C.H. Chung, M.A. Perillo, Y.C. Chang, H. Koo, Z. Zheng, C.S. Li, The impact of dental implant surface modifications on osseointegration and biofilm formation. J. Clin. Med. **10**(8), 1641 (2021)
35. E. Guibal, Interactions of metal ions with chitosan-based sorbents: a review. Sep. Purif. Technol. **38**(1), 43–74 (2004)
36. A. Radornska-Soukharev, Stability of lipid exciplents in solid lipid nanoparticles. Adv. Drug Deliver. Rev. **59**(6), 411–418 (2007)
37. Y. Cheng, X. Luo, J. Betz, S. Buckhout-White, O. Bekdash, G.F. Payne, W.E. Bentley, G.W. Rubloff, In situ quantitative visualization and characterization of chitosan electrodeposition with paired sidewall electrodes. Soft Matter **6**(14), 3177–3183 (2010)
38. M. Mishra, S. Bhattacharjee, L. Besra, H.S. Sharma, T. Uchikoshi, Y. Sakka, Effect of pH localization on microstructure evolution of deposits during aqueous electrophoretic deposition (EPD). J. Eur. Ceram. Soc. **30**(12), 2467–2473 (2010)
39. A.P. Abbott, K.J. McKenzie, Application of ionic liquids to the electrodeposition of metals. Phys. Chem. Chem. Phys. **8**(37), 4265–4279 (2006)
40. V. Karageorgiou, D. Kaplan, Porosity of 3D biomaterial scaffolds and osteogenesis. Biomaterials **26**(27), 5474–5491 (2005)
41. P. Huang, K. Ma, X. Cai, D. Huang, X. Yang, J. Ran, F. Wang, T. Jiang, Enhanced antibacterial activity and biocompatibility of zinc-incorporated organic-inorganic nanocomposite coatings

via electrophoretic deposition. Colloid. Surface. B **160**, 628–638 (2017)
42. S.Z. Li, H. Zhang, J. Xu, D. Yang, Hydrothermal synthesis of flower-like SrCO3 nanostructures. Mater. Lett. **59**(4), 420–422 (2005)
43. W. Hu, S. Chen, X. Li, S. Shi, W. Shen, X. Zhang, H. Wang, In situ synthesis of silver chloride nanoparticles into bacterial cellulose membranes. Mater. Sci. Eng. C Mater. Bio. Appl. **29**(4), 1216–1219 (2009)
44. Y. Herdiana, N. Wathoni, S. Shamsuddin, M. Muchtaridi, Drug release study of the chitosan-based nanoparticles. Heliyon **8**(1), e08674 (2022)
45. M. Goldberg, R. Langer, X.Q. Jia, Nanostructured materials for applications in drug delivery and tissue engineering. J. Biomat. Sci.-Polym. E. **18**(3), 241–268 (2007)
46. R.A. Petros, J.M. DeSimone, Strategies in the design of nanoparticles for therapeutic applications. Nat. Rev. Drug Discov. **9**(8), 615–627 (2010)
47. Y.J. Kuo, C.H. Chen, P. Dash, Y.C. Lin, C.W. Hsu, S.J. Shih, R.J. Chung, Angiogenesis, osseointegration, and antibacterial applications of polyelectrolyte multilayer coatings incorporated with silver/strontium containing mesoporous bioactive glass on 316L stainless steel. Front. Bioeng. Biotech. **10**, 818137 (2022)
48. R.O. Darouiche, Current concepts—treatment of infections associated with surgical implants. N. Engl. J. Med. **350**(14), 1422–1429 (2004)
49. V. Sambhy, M.M. MacBride, B.R. Peterson, A. Sen, Silver bromide nanoparticle/polymer composites: dual action tunable antimicrobial materials. J. Am. Chem. Soc. **128**(30), 9798–9808 (2006)
50. M. Rai, A. Yadav, A. Gade, Silver nanoparticles as a new generation of antimicrobials. Biotechnol. Adv. **27**(1), 76–83 (2009)
51. A.S. Kazachenko, E.V. Legler, O.V. Per'yanova, Y.A. Vstavskaya, Synthesis and antimicrobial activity of silver complexes with histidine and tryptophan. Khim.-Farm. Zh. **34**(5), 34–35 (2000)
52. O. Choi, K.K. Deng, N.-J. Kim, L. Ross Jr., R.Y. Surampalli, Z. Hu, The inhibitory effects of silver nanoparticles, silver ions, and silver chloride colloids on microbial growth. Water Res. **42**(12), 3066–3074 (2008)
53. J. Braux, F. Velard, C. Guillaume, S. Bouthors, E. Jallot, J.M. Nedelec, D. Laurent-Maquin, P. Laquerriere, A new insight into the dissociating effect of strontium on bone resorption and formation. Acta Biomater. **7**(6), 2593–2603 (2011)
54. L. Zhao, H. Wang, K. Huo, X. Zhang, W. Wang, Y. Zhang, Z. Wu, P.K. Chu, The osteogenic activity of strontium loaded titania nanotube arrays on titanium substrates. Biomaterials **34**(1), 19–29 (2013)